Hindawi Publishing Corporation
Advances in Physical Chemistry
Volume 2011, Article ID 821204, 8 pages
doi:10.1155/2011/821204

Research Article

N-TiO_2: Chemical Synthesis and Photocatalysis

Matias Factorovich,[1] Lucas Guz,[2] and Roberto Candal[1,2]

[1] *INQUIMAE-CONICET, Facultad de Ciencias Exactas y Naturales, Universidad de Buenos Aires, Ciudad Universitaria, Pabellón II, 1428 Buenos Aires, Argentina*
[2] *Escuela de Ciencia y Tecnología, 3iA, Universidad Nacional de San Martín, Campus Miguelete, 1650 San Martín, Prov. de Buenos Aires, Argentina*

Correspondence should be addressed to Roberto Candal, rjcandal@gmail.com

Received 29 September 2011; Revised 17 November 2011; Accepted 17 November 2011

Academic Editor: Taicheng An

The chemical synthesis of nitrogen-doped titanium dioxide (N-TiO_2) is explored in an attempt to understand the mechanisms of doping. Urea is used as precursor in a sol gel synthesis of N-TiO_2. Chemical and structural changes during thermal treatment of the precursors were followed by several techniques. The effect of doping on band gap, morphology, and microstructure was also determined. The byproducts produced during firing correspond to those obtained during urea thermal decomposition. Polynitrogenated colored compounds produced at temperatures below 400°C may act as sensitizer. Incorporation of N in the TiO_2 structure is possible at higher temperatures. Degradation experiments of salicylic acid under UVA and visible light ($\lambda > 400$ nm) in the presence of TiO_2 or N-TiO_2 indicate that doping decreases the activity under UVA light, while stable byproducts are produced under visible light.

1. Introduction

The development of novel materials capable of solar-driven chemical transformation or electricity production is one of the more important challenges for now and the following years. Oxide semiconductors are an interesting family of semiconductors that can use solar light to catalyze several chemical processes and/or produce electricity. In this sense, TiO_2 is a noble material due to its chemical stability, photocorrosion resistance, and low toxicity [1, 2]. However, TiO_2 can absorb only the relatively small part of the solar spectrum that includes the $300 < \lambda < 390$ nm range (around 5% of the solar light). In an attempt to improve light absorption in the visible range, TiO_2 was modified by incorporation of transition metals, noble metals and recently by nonmetallic elements [3–7].

During recent years, N-TiO_2 became one of the more studied nonmetal-doped systems. The presence of a nontoxic dopant and the reported activity are the principal reasons why N-TiO_2 is chosen as a promising photocatalyst to be used under solar light illumination.

The methods to prepare N-TiO_2 can be summarized as follows:

(1) sputtering and implantation techniques [8–10]: these techniques are adequate for the preparation of films;

(2) calcinations of TiO_2 or $Ti(OH)_4$ under N-containing atmospheres generated by nitrogen compounds like ammonia [11–13]: these techniques are principally used to prepare powders;

(3) sol-gel process [5, 14–16] which can be used to prepare powders or films.

The preparation method has an important role in determining the final properties of the products, because different ways to incorporate N lead to systems with dopant located in different positions of the TiO_2 structure and with different activities [15, 17, 18].

N-TiO_2 can be synthesized by chemical method if an appropriate N containing precursor is selected. This methodology is attractive because there is no expensive equipment involved, which helps to reduce costs for the massive

synthesis of the product. Coprecipitation of TiO_2 with urea followed by thermal treatment is one of the most popular procedures to prepare N-TiO_2 [14, 19, 20]. However, the mechanism of doping is still not well understood and is a challenge for chemists to determine how TiO_2 is doped by N under those conditions. Besides, the synthesis is sometimes difficult to reproduce; so a better understanding of the process is necessary in order to develop reliable synthesis.

In this paper, we present the results of studies designed to understand the mechanisms involved in the synthesis and in the determination of the photocatalytic activity of the materials under black and white light illumination.

2. Materials and Methods

2.1. N-TiO_2 Synthesis and Characterization. The synthesis procedure is based on what was reported by Ohno [19]. Three solutions containing Ti-isopropoxide, $Ti(C_3H_7O)_4$ (Aldrich), urea (Anedra PA), or water dissolved in absolute ethanol (Merck, PA) were prepared: solution (a) $Ti(C_3H_7O)_4$ 0.40 mol dm^{-3}, solution (b) urea 0.80 mol dm^{-3}, and solution (c) water 0.40 mol dm^{-3}. Solution (a) was incorporated into solution (b) under stirring and mixed during 15 minutes. After the stirring period, solution (c) was slowly incorporated to the mixture under stirring. A white slurry was obtained, which was stirred for another 60 minutes. Finally, the slurry was evaporated under vacuum at 40°C until a white precursor powder, with a 4 : 1 N : Ti molar ratio, was obtained. In order to determine the effect of N doping on microstructure, precursor powders with N : Ti ratios 2 : 1 and 8 : 1 were prepared following the same protocol, but using solutions (b) with 0.40 and 1.6 mol dm^{-3} urea, respectively. The product was air-dried and fired under air at 175, 250, 375, 412, 450, or 500°C, during 15 min with a 10°C/min ramp. The precursor powders used in photocatalysis experiments and those with N : Ti ratios 2 : 1 and 8 : 1 were fired at 250°C for 3 h, heated to 500°C with a 10°C/min ramp, and immediately cooled down in the oven. Finally, they were washed with water to remove possible soluble impurities and dried at 60°C. As control, pure TiO_2 was synthesized in a similar way, but without the incorporation of urea.

The evolution of the powder precursor during firing was followed by thermal gravimetric analysis (TGA; Shimadzu TG-50) and differential thermal analysis (DTA; Shimadzu DTA-50) under air atmosphere. The nature of the byproducts obtained at the different firing temperatures was determined by Fourier transformed infrared spectroscopy (FTIR, Thermo Nicolet 8700). The crystalline phases predominant at each temperature were determined by X-ray diffraction (XRD; Siemens D-5000) using the Cu Kα wavelength. The bandgap of the different samples was determined by reflectance spectroscopy (Shimadzu UV-3101PC), using $BaSO_4$ as reference. Surface area and porosity of the powders were measured by N_2 sorptometry, using the BET formalism (Micromeritics ASAP 2020 V3.00 H). The morphology of the particles of powders was determined by Field Emission Scanning Electron Microscopy (FEGSEM Zeiss LEO 982 GEMINI).

2.2. Photocatalytic Activity. The photocatalytic activity of the different photocatalysts was determined through the degradation of salicylic acid (Fluka, PA, USA) as model contaminant. Salicylic acid is a nice target because the presence of aromatic and phenol functionality, with negligible toxicity at the used concentrations (2.5×10^{-4} M). A homemade photoreactor was used for all the experiments. A borosilicate glass cylindrical container (200 mL) was surrounded by four 12 W light tubes, symmetrically placed at 15 cm from the axis of the cylinder. The photocatalyst was incorporated to the salicylic acid solution and suspended with the application of ultrasound for 10 minutes. The final concentration of photocatalyst was 1.0 g/L. The suspension was magnetically stirred, and O_2 was bubbled during all the experiment. The system was stirred in the dark during 30 minutes to reach adsorption equilibrium. The lamps were warmed up during 15 minutes. Once the reactor was under illumination, 5 mL samples were taken at regular periods. The samples were filtered through a 0.45 μm pore diameter polycarbonate membrane (Sartorius) and stored in glass containers at −20°C until analysis was performed.

The experiments run under UVA light were carried out using 12 W black light tubes, while for the experiments with visible light 12 W, white tubes were used. In the latter case, a 4 mm thick Plexiglas cylinder was placed surrounding the borosilicate glass reactor to eliminate all the emissions with wavelength lower than 400 nm. The intensity of light inside the photoreactor was determined with a radiometer at 360 nm, using a combination of two filters: WG 335 and UG 11. The radiance was calculated through:

$$\frac{\text{Photons}}{\text{s} \cdot \text{cm}^2} = \frac{\text{P}}{\text{A} \cdot \text{E}} \cdot \text{f}, \tag{1}$$

where P is luminic potency; A is photodiode area; E is photon energy (hν/360 nm); h is Planck's constant; f is correction factor due to filter attenuation (f = 13.43).

The concentration of the remaining salicylic acid in the irradiated samples was determined by High-Performance Liquid Chromatography (HPLC), Shimadzu, equipped with an Econosphere C-18, 150 mm × 4 mm, column, and UV-Vis detector. The solvent carrier was a 25 : 75 methanol:acetic acid (2% in water), with a flow rate of 1.4 mL/min. Salicylic acid was detected at 298 nm. To detect the presence of byproducts, standards of dihydroxybenzoic acid and hydroquinone were analyzed by HPLC with UV detection.

3. Results

Figures 1(a), 1(b) and, 1(c) show TGA and DTA plots of urea, TiO_2 powder, and coprecipitated TiO_2-urea powder, respectively. As shown in Figure 1(a), decomposition of pure urea starts after melting, characterized by a sharp endothermic peak at 133°C, with a steep loss of mass that involves at least two processes, as indicated by the endothermic peaks at 191 and 230°C. There is a small plateau in the 260–300°C range, followed by another steep loss of mass that ends at 360°C and corresponds with one endothermic process centered at 330°C. Finally, there is another endothermic process centered at 395°C, associated with a smooth loss of mass in the

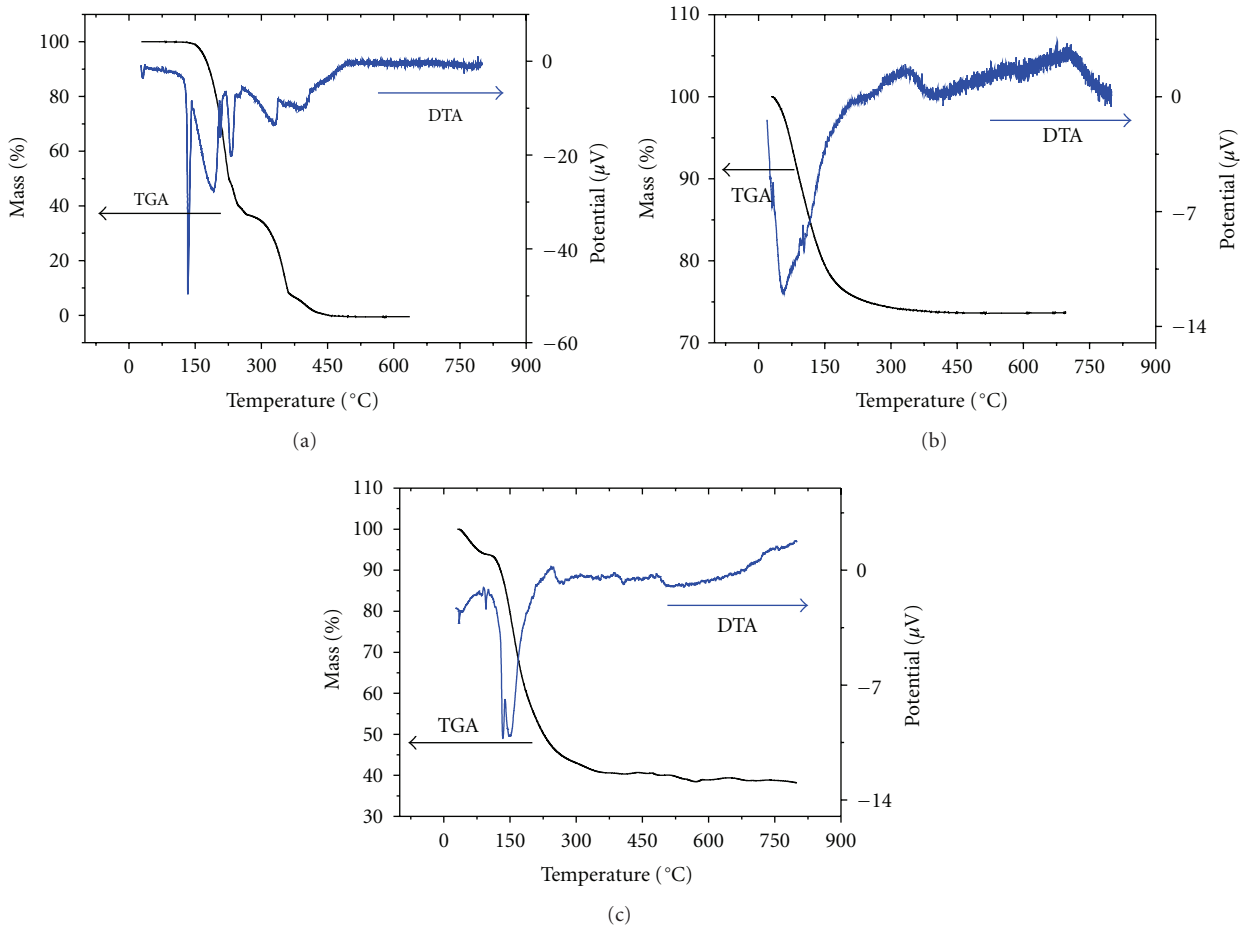

Figure 1: TGA (left vertical axe) and DTA (right vertical axe) analysis of samples: (a) urea, (b) TiO_2, and (c) TiO_2 + urea (N : Ti, 4 : 1).

range 330–450°C. In the case of pure TiO_2, synthesized as explained previously, the thermal behavior is much simpler. There is a steep loss of mass in the range 33–300°C that corresponds with a broad endothermic process that likely contains, at least, two superimposed processes centered at 56 and 110°C. The coprecipitated mix of urea and TiO_2 displays similar behavior to pure TiO_2. As shown in Figure 1(c), mass is lost from the beginning of the heating, with a steep loss at 115°C. The slope of the curve decreases as the temperature rises. DTA indicates that decomposition starts immediately after urea melting (133°C); probably the different processes observed in Figure 1(a) are superimposed in the peak centered at 150°C in Figure 1(c). It should be considered that the mass of urea is lower than in the experiment shown in Figure 1(a), because in the case of Figure 1(c), there is a mixture of urea and TiO_2. Consequently, some processes that involve small losses of mass may be hidden.

Figure 2 shows FTIR spectra of raw coprecipitated TiO_2-urea and fired at different temperatures. As can be seen in the figure, the raw mixture displays the typical features of urea corresponding to N-H stretching (3450 and 3300 cm^{-1}), C=O (1600 cm^{-1}), and N-C (1340–1250 cm^{-1}) [21]. After firing at different temperatures, new features can be characterized and others disappear. The more important changes

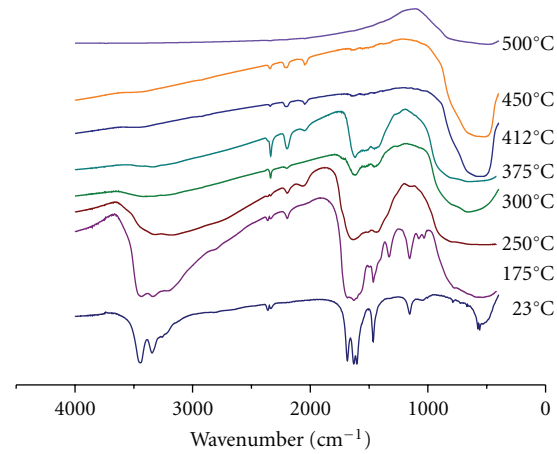

Figure 2: FTIR spectra of TiO_2-urea (N : Ti, 4 : 1) samples fired at the indicated temperature during 10 minutes. Heating ramp: 10°C/min. Samples were cooled down to room temperature in the oven.

take place in two ranges: 175–375°C and 375–500°C. In the first range, the typical peaks of urea are replaced by others typical of biuret (see also Figure 7), (1405 cm^{-1}, 1330 cm^{-1},

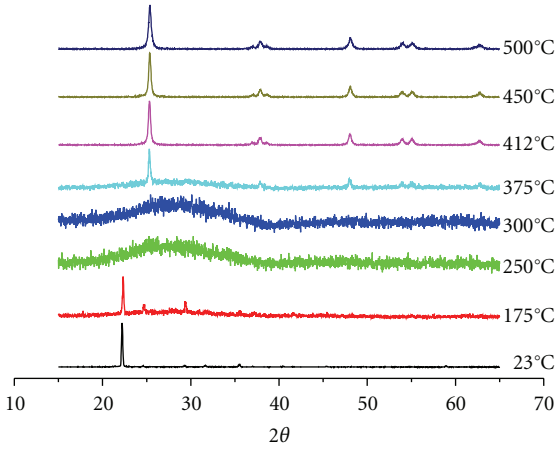

Figure 3: XRD patterns of TiO_2-urea (N : Ti, 4 : 1) samples fired at the indicated temperature during 10 minutes. Heating ramp: 10°C/min. Samples were cooled down to room temperature in the oven.

Table 1: Surface area, pore volume, and pore size of samples prepared from precursors with different N : Ti molar ratios, fired at 250°C, 3 h, and 500°C 1 min. Ramp: 10°C/min.

Sample	Surface area m^2/g	Pore volume cm^3/g	Pore size Å
N : Ti, 0 (TiO_2)	52	0.088	66
N : Ti, 2 : 1	40	0.068	56
N : Ti, 4 : 1	26	0.051	63
N : Ti, 8 : 1	17	0.034	64

1075 cm^{-1}, and 1025 cm^{-1}), cyanuric acid (1158 cm^{-1}), ammelide, ammeline, and melanine with typical bands in the 1800–1300 cm^{-1} range among others (see [22] and references cited therein). There are also bands at 2048, 2195, and 2340 cm^{-1} that correspond with cyanides and cyanates; these bands increase as the other decrease with the temperature. In the range 412–500°C, only the bands typical of cyanates and cyanides remain in the spectra in the range 3500–1000 cm^{-1}, and the bands corresponding to O-Ti-O stretching, in the range 400–600 cm^{-1}, increase with the temperature.

Figure 3 shows X-Ray diffractograms of TiO_2-urea coprecipitated samples fired at different temperatures. The raw sample displays features that correspond to crystalline urea. As the temperature increases, the peaks become less intense, until in the range 250–300°C the samples are noncrystalline. At 375°C, the sample is slightly crystalline, while at higher temperatures, it becomes crystalline. Anatase is the only crystalline phase present in the range 375–500°C. It is noteworthy that when the solid starts to crystallize, polynitrogenated cyclic compounds, such as ammelide, ammeline, and melanine are present on the TiO_2 particles, as determined by FTIR (see Figure 2).

Figure 4 shows SEM images of pure TiO_2 and N-TiO_2 samples prepared from different N : Ti ratios. In all the cases, the particles that form the aggregates are nanometric, with an average size of approximately 10 nm. As the urea/Ti ratio increases, the morphology of the systems notably changes. The particles seem bigger and the porosity decreases. The N_2 sorption experiments displayed in Table 1 agree with the SEM images. The surface area and the pore volume decrease as the urea/Ti ratio in the synthesis increases.

Figure 5 shows the reflectance spectra and the band gap of TiO_2, N-TiO_2, and a commercial sample (Finnit by Kemira). The remission function was calculated from the reflectance data through the Kubelka-Munk function:

$$F(R) = \frac{(1-R)^2}{2R}, \tag{2}$$

where $F(R)$ is the remission function and R is the measured reflectance.

The band-gap energy can be obtained by extrapolation to zero of a plot of $(F(R) \times E)^{1/2}$ versus E, where E is the energy of the incident light in eV. The band gap of the commercial sample corresponds with anatase (3.26 eV). The TiO_2 synthesized in the laboratory has a band gap shifted to lower energies, compared with pure anatase. N-TiO_2 displays a shoulder at 2.5–2.7 eV, which can be associated with the deep yellow color displayed by the N-doped samples.

Analysis of the surface chemical composition by XPS shown in Table 2 indicates the presence of N in all the studied samples. The presence of N in the bare TiO_2 sample can be assigned to physisorbed N (400.9 eV). The concentration of N increases with the urea/Ti ratio. The binding energies can be assigned to substitutional N (396-397 eV), interstitial N (400 eV) [18], graphite-like phases: (400.6 eV, N-Csp^2), or polycyanogen (399.0–400.5 eV, $(\text{-C=N-})_x$) [23], due to polycyclic nitrogenated compounds. Table 2 also shows that C is present in all the samples.

Photocatalytic activity of TiO_2 and N-TiO_2 was determined under UVA (360 nm) and visible light ($\lambda \geq 400$ nm). When black lights were used, the photon flux at 360 nm inside the reactor was 1.67×10^{16} photons/(s cm^2). In the case of white lamps, the 360 nm emission was removed by the Plexiglas filter; the photon flux at different wavelength was 4.65×10^{15} (400 nm), 1.37×10^{16} (436 nm), 1.19×10^{16} (492 nm), 2.22×10^{16} (547 nm), and 1.77×10^{16} photons/(s cm^2) (579 nm). As the band-gap energy for TiO_2 synthesized in the laboratory is 3.03 eV and for N-TiO_2 is 2.38 eV, only the emissions with wavelengths shorter than 400 or 547 nm can be, respectively, absorbed by the photocatalysts.

Salicylic acid was used as target contaminant; Figure 6(a) shows the temporal evolution of the concentration when a 2.5×10^{-4} M solution containing 1.0 g/L of catalyst is illuminated with black or white light. Under UVA illumination, N-TiO_2 displayed much lower efficiency than TiO_2 synthesized under similar conditions. Under visible light, N-TiO_2 was slightly more efficient than TiO_2 and, in both cases, the degradation rate decreases with the time. Figure 6(b) shows the concentration of dihydroxybenzoic acid (DHB) relative to the remnant salicylic acid at different illumination times. It is clear that the highest accumulation of DHB is observed with N-TiO_2, followed by TiO_2, in both cases under visible light. Direct photolysis of salicylic acid by UVA illumination, as shown in Figure 6(a), or visible light illumination (not shown) was negligible during the studied period. Adsorption

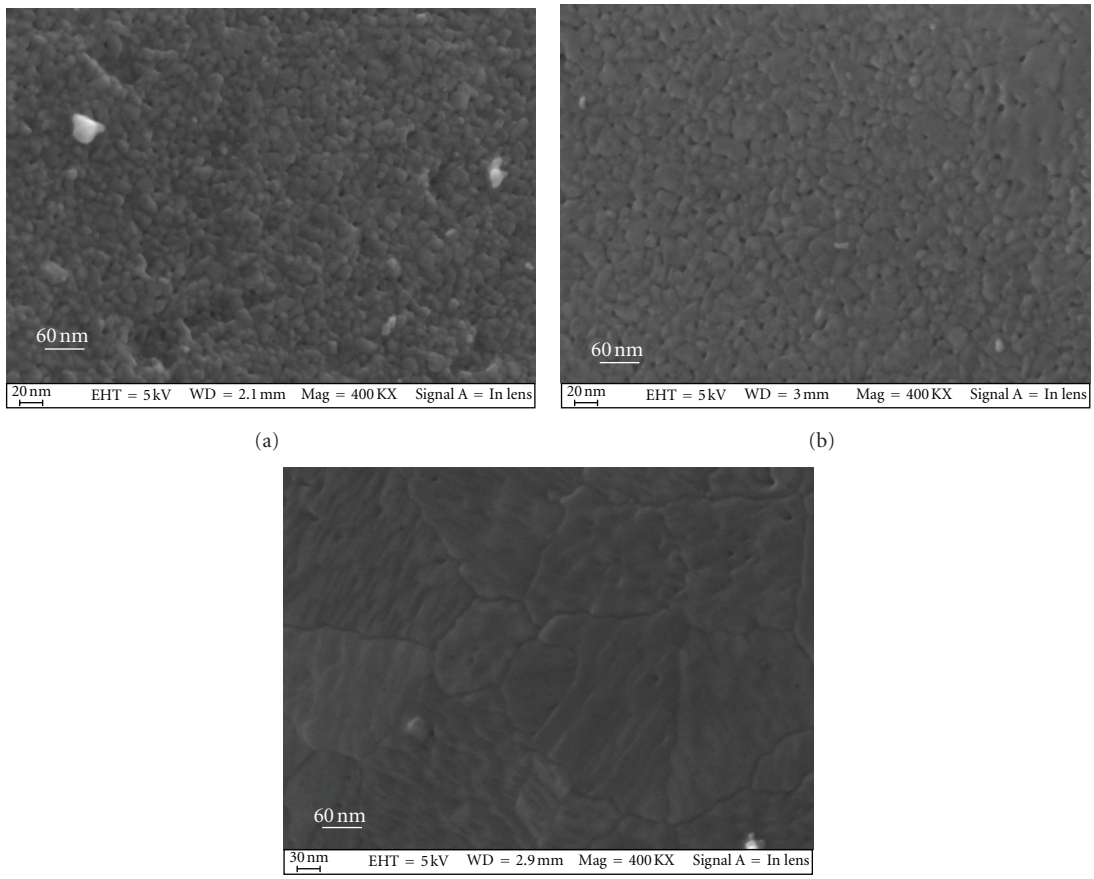

Figure 4: SEM images of N-TiO_2 samples prepared from precursors with different N : Ti molar ratios, fired at 250°C, 3 h, and 500°C 1 min. Ramp: 10°C/min. (a) N : Ti, 0 (TiO_2); (b) N : TI, 4 : 1; (c) N : Ti, 8 : 1.

Table 2: Surface % at/at for Ti, O, C, and N determined by XPS. Samples are prepared from precursors with different N : Ti molar ratios, fired at 250°C, 3 h, and 500°C 1 min. Ramp: 10°C/min.

Sample	Titanium%	Oxygen%	Carbon%	Nitrogen%	N/Ti × 100%
TiO_2 N : Ti, 0	24	63	11	1.7	7.0
N-TiO_2 N : Ti, 4 : 1	24	62	10	4.0	17
N-TiO_2 N : Ti, 8 : 1	22	59	15	3.9	18

of salicylic acid on TiO_2 and N-TiO_2 was 12–25% of the initial concentration.

4. Discussion

The transformation of the coprecipitated urea-TiO_2 system during thermal treatment starts after the melting of urea, as can be seen in Figures 1(c) and 2. The byproducts detected in samples fired at different temperatures are coincident with that reported by Schaber et al. [22]. The decomposition reaction begins with the condensation of urea yielding biuret. Figure 7 compares FTIR spectra of urea, biuret, and a sample fired at 175°C. Clearly, the sample contains both urea and biuret as shown by the characteristic peaks indicated with arrows "u" or "b," respectively. The heating at higher temperatures produces further condensation leading to more complex polynitrogenated compounds as melamine. Cyanates and cyanides are also present in the fired samples. It can be noticed in Figure 2 that as the temperature increases, the intensity of the features corresponding to polynitrogenated compounds (1300–1800 cm^{-1}) decreases in comparison with those of cyanates and cyanides (2048–2340 cm^{-1}). As the firing temperature gets close to 500°C, all the features disappear and eventually the samples become white. The synthesis of polynitrogenated compounds on the surface of TiO_2 can be a consequence of the condensation

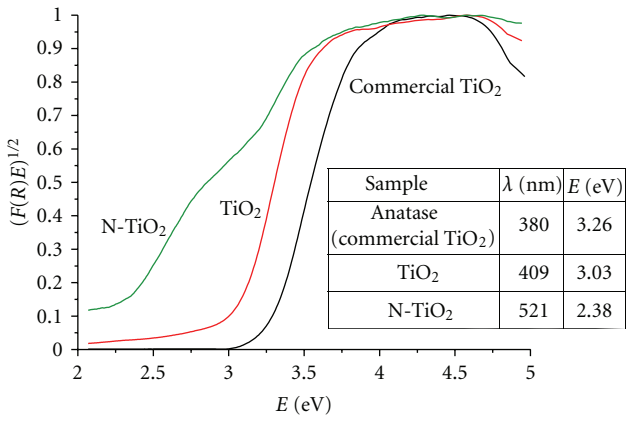

FIGURE 5: Plot of the product $[F(R) \times E]^{1/2}$ versus E, where $F(R)$ is the remission function, and E is the energy in eV, for different samples. The band-gap values of each sample, determined by extrapolation of the lineal part of the plot until intersection with the E axe, are shown in the inset.

reaction as postulated by Mitoraj and Kisch [23, 24], which starts with the synthesis of melamine:

$$\equiv \mathrm{Ti}-\mathrm{OH} + \mathrm{O}=\mathrm{C}=\mathrm{N}-\mathrm{H} \longrightarrow \equiv \mathrm{Ti}-\mathrm{OH}-\mathrm{CO}-\mathrm{NH} \quad \equiv \mathrm{Ti}-\mathrm{NH}_2 + \mathrm{CO}_2$$

$$\equiv \mathrm{Ti}-\mathrm{NH}_2 + \mathrm{H}-\mathrm{O}-\mathrm{C}\equiv\mathrm{N} \longrightarrow \equiv \mathrm{Ti}-\mathrm{OH} + \mathrm{H}_2\mathrm{N}-\mathrm{C}\equiv\mathrm{N}$$

$$6(\mathrm{NH}_2)_2\mathrm{CO} \longrightarrow \mathrm{C}_3\mathrm{H}_6\mathrm{N}_6 + 6\mathrm{NH}_3 + 3\mathrm{CO}_2$$

Further condensation of melamine leads to melam, melon, and so forth. All these compounds are dyes that withstand temperatures close to 400°C, which turn the N-TiO$_2$ system yellow. The presence of these compounds or their firing byproducts may be responsible of the reduction of surface area in the N-TiO$_2$ samples, as indicated in Table 1 and Figure 4.

Crystallization begins in the range 300–375°C, where polynitrogenated compounds are still present in the samples. N may be incorporated into the TiO$_2$ structure as the samples crystallize with the increase of the firing temperature. Buha et al. reported that nitrides can be formed from oxides by thermal treatment in the presence of urea or cyanamide at 800 C [25]. The conversion to titanium nitride is total with 5 nm TiO$_2$ particles, while for 20 nm particles titanium nitride and titanium oxide coexist. The particle size of the systems studied in this work is close to 20 nm; so based on the previous report, the substitution of oxides by nitrides seems to be possible.

The incorporation of N into the TiO$_2$ structure might explain the shift in the band gap determined by diffuse reflectance (Figure 5). Carbon can also act as a dopant, helping in the shift of the band gap to lower energy. It should be noticed that in the TiO$_2$ sample synthesized following a similar procedure as for N-TiO$_2$ the band gap is lower than in pure anatase. Carbon doping can be the reason of the band-gap shift in this case. Figure 5 shows a shoulder in the visible range, which indicates the presence of surface or intraband-gap states in the samples. Mitoraj et al. [26] proposed that nitrogen-carbon-doped TiO$_2$ (N,C-TiO$_2$) displays an energy band-like structure of intraband-gap states, while N-TiO$_2$ has a manifold of discrete levels. Hole (h^+) stabilization by charge delocalization is more likely in N,C-TiO$_2$. Our results do not allow to discriminate between doping or sensitization produced by the polynitrogenated dyes, but it is clear that both effects are related with the band-gap shift and the shoulder observed by diffuse reflectance in the visible range.

The photocatalytic activity of TiO$_2$ is notably affected by doping as shown in Figure 6. N-TiO$_2$ under UVA light displays the lowest activity for the degradation of salicylic acid, while TiO$_2$ displays the highest. The presence of surface states may enhance hole electron recombination in N-TiO$_2$ leading to low activity. When visible light was used in the experiments, degradation of salicylic acid was observed with both photocatalysts. The degradation rate notably decreases after 250 minutes and almost stops completely in the case of N-TiO$_2$. Figure 6(b) shows that DHB acid was detected in these experiments and that its concentration, relative to the remnant salicylic concentration, was higher than in other cases. When the system is illuminated with visible light, the polynitrogenated compounds inject electrons into the TiO$_2$ conducting band, generating excited dye radicals on the surface. Górska et al. proposed that in N,C-TiO$_2$, superoxide radicals or direct charge transfer to the adsorbed organic are involved in degradation paths [27]. The oxidation power of these species is lower than that of $OH^\bullet$ or h^+, leading to less oxidized byproducts which can poisoned the surface of the catalyst.

The degradation of salicylic acid on TiO$_2$ can be a consequence of C doping, which shifts the band gap to 3.03 eV, allowing the absorption of light with 400 nm wavelength. The light source has a moderate emission at 400 nm which can be used to activate the catalyst. However, another effect should be considered. Salicylic acid can be absorbed on the TiO$_2$ surface in the form of different surface complexes [28]. These complexes display an absorption band in the visible range and can act as sensitizers of TiO$_2$ [29], leading to the self-degradation of salicylic acid. Both phenomena may be responsible for the target degradation, and it is not possible to discriminate which is the most important.

5. Conclusions

Byproducts generated during urea thermal decomposition are key in the synthesis of N-TiO$_2$. Some byproducts, such as biuret, might be used as precursors themselves. Sol-gel synthesis with urea as N-precursor leads to the production of crystalline N-TiO$_2$ sensitized with polycyclic nitrogen compounds at firing temperatures lower than 400 C. At firing temperatures higher than 400 C, N doping is related with the presence of simpler nitrogenated species or N incorporation. N-TiO$_2$ photocatalytic activity is higher under *vis* light than under UVA illumination. Accumulation of byproducts was detected in TiO$_2$ and N-TiO$_2$ systems illuminated with white light. Target compounds chemisorbed on TiO$_2$ surface can be degraded by *vis* light. Both phenomena may by superimposed in N-TiO$_2$ photocatalysis.

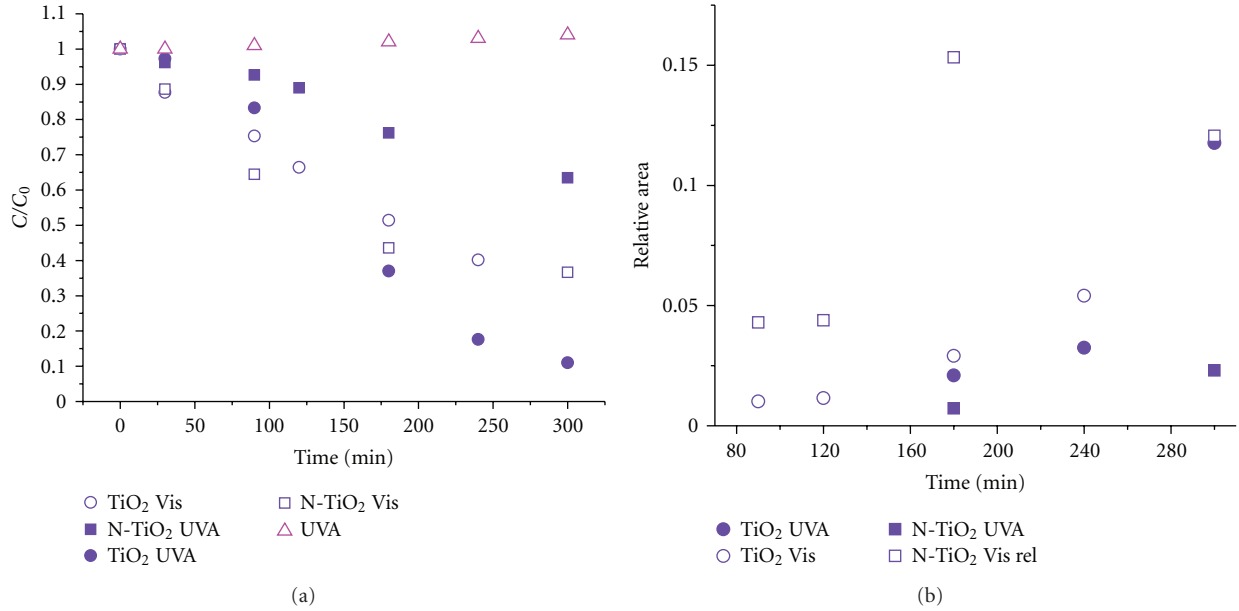

FIGURE 6: (a) Evolution of salicylic acid concentration versus irradiation time, in solution containing 2.5×10^{-4} M salicylic acid and 1.0 g/L of photocatalyst. UVA and Vis correspond to experiments performed under black light (360 nm) or filtered white light ($\lambda > 400$ nm), respectively. (b) Evolution of DHB/salicylic ratio versus irradiation time for different catalysts and light (DHB: dihydroxybenzoic acid). TiO_2 and N-TiO_2 samples are prepared from precursors with N : Ti, 0 and N : Ti, 4 : 1, respectively, fired at 250°C, 3 h, and 500°C 1 min. Ramp: 10°C/min.

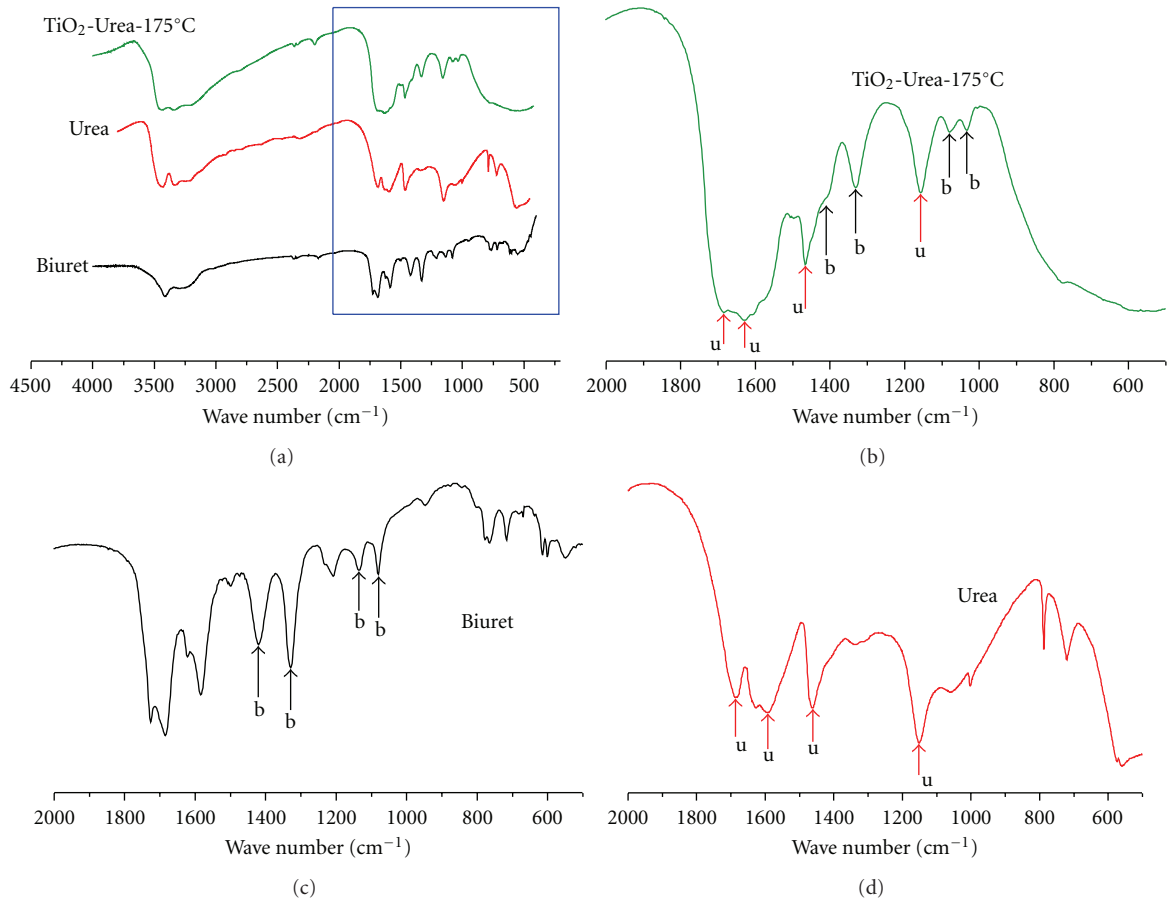

FIGURE 7: FTIR spectra of urea, biuret, and a sample of urea-TiO_2 (N : Ti, 4 : 1) fired at 175°C.

Acknowledgments

The authors acknowledge funding given by University of Buenos Aires (Projects X411 and 20020090100297) and University of San Martín (UNSAM SA08/011). R. Candal is Member of CONICET. CONICET fellowship given to L. Guz is gratefully thanked. They thank Dr. L. Tribe for her help with English.

References

[1] S. Y. Lu, D. Wu, Q. L. Wang, J. Yan, A. G. Buekens, and K. F. Cen, "Photocatalytic decomposition on nano-TiO_2: destruction of chloroaromatic compounds," *Chemosphere*, vol. 82, pp. 1215–1224, 2011.

[2] S. Malato, P. Fernández-Ibáñez, M. I. Maldonado, J. Blanco, and W. Gernjak, "Decontamination and disinfection of water by solar photocatalysis: recent overview and trends," *Catalysis Today*, vol. 147, no. 1, pp. 1–59, 2009.

[3] M. Ni, M. K. H. Leung, D. Y. C. Leung, and K. Sumathy, "A review and recent developments in photocatalytic water-splitting using TiO_2 for hydrogen production," *Renewable and Sustainable Energy Reviews*, vol. 11, no. 3, pp. 401–425, 2007.

[4] S. Rehman, R. Ullah, A. M. Butt, and N. D. Gohar, "Strategies of making TiO_2 and ZnO visible light active," *Journal of Hazardous Materials*, vol. 170, no. 2-3, pp. 560–569, 2009.

[5] U. G. Akpan and B. H. Hameed, "The advancements in sol-gel method of doped-TiO_2 photocatalysts," *Applied Catalysis A*, vol. 375, no. 1, pp. 1–11, 2010.

[6] J. Zhang, Y. Wu, M. Xing, S. A. K. Leghari, and S. Sajjad, "Development of modified N doped TiO_2 photocatalyst with metals, nonmetals and metal oxides," *Energy and Environmental Science*, vol. 3, no. 6, pp. 715–726, 2010.

[7] C. M. Teh and A. R. Mohamed, "Roles of titanium dioxide and ion-doped titanium dioxide on photocatalytic degradation of organic pollutants (phenolic compounds and dyes) in aqueous solutions: a review," *Journal of Alloys and Compounds*, vol. 509, no. 5, pp. 1648–1660, 2011.

[8] K. G. Grigorov, I. C. Oliveira, H. S. MacIel et al., "Optical and morphological properties of N-doped TiO_2 thin films," *Surface Science*, vol. 605, no. 7-8, pp. 775–782, 2011.

[9] S. M. Marques, C. J. Tavares, L. F. Oliveira, and A. M. F. Oliveira-Campos, "Photocatalytic degradation of C.I. Reactive Blue 19 with nitrogen-doped TiO_2 catalysts thin films under UV/visible light," *Journal of Molecular Structure*, vol. 983, no. 1–3, pp. 147–152, 2010.

[10] L. Jinlong, M. Xinxin, S. Mingren, X. Li, and S. Zhenlun, "Fabrication of nitrogen-doped mesoporous TiO_2 layer with higher visible photocatalytic activity by plasma-based ion implantation," *Thin Solid Films*, vol. 519, no. 1, pp. 101–105, 2010.

[11] M. Janus and A. W. Morawski, "New method of improving photocatalytic activity of commercial Degussa P25 for azo dyes decomposition," *Applied Catalysis B*, vol. 75, no. 1-2, pp. 118–123, 2007.

[12] M. Janus, J. Choina, and A. W. Morawski, "Azo dyes decomposition on new nitrogen-modified anatase TiO_2 with high adsorptivity," *Journal of Hazardous Materials*, vol. 166, no. 1, pp. 1–5, 2009.

[13] Y. Wang, C. Feng, M. Zhang, J. Yang, and Z. Zhang, "Enhanced visible light photocatalytic activity of N-doped TiO_2 in relation to single-electron-trapped oxygen vacancy and doped-nitrogen," *Applied Catalysis B*, vol. 100, no. 1-2, pp. 84–90, 2010.

[14] M. Chekini, M. R. Mohammadizadeh, and S. M. Vaez Allaei, "Photocatalytic and superhydrophilicity properties of N-doped TiO_2 nanothin films," *Applied Surface Science*, vol. 257, no. 16, pp. 7179–7183, 2011.

[15] C. Cantau, T. Pigot, J. C. Dupin, and S. Lacombe, "N-doped TiO_2 by low temperature synthesis: stability, photo-reactivity and singlet oxygen formation in the visible range," *Journal of Photochemistry and Photobiology A*, vol. 216, no. 2–4, pp. 201–208, 2010.

[16] M. Qiao, Q. Chen, S. Wu, and J. Shen, "Novel sol-gel synthesis of N-doped TiO_2 hollow spheres with high photocatalytic activity under visible light," *Journal of Sol-Gel Science and Technology*, vol. 55, no. 3, pp. 377–384, 2010.

[17] D. Meroni, S. Ardizzone, G. Cappelletti et al., "Photocatalytic removal of ethanol and acetaldehyde by N-promoted TiO_2 films: the role of the different nitrogen sources," *Catalysis Today*, vol. 161, no. 1, pp. 169–174, 2011.

[18] C. Di Valentin, E. Finazzi, G. Pacchioni et al., "N-doped TiO_2: theory and experiment," *Chemical Physics*, vol. 339, no. 1-3, pp. 44–56, 2007.

[19] T. Ohno, "Preparation of visible light active S-doped TiO_2 photocatalysts and their photocatalytic activities," *Water Science and Technology*, vol. 49, no. 4, pp. 159–163, 2004.

[20] J. Nieto, J. Freer, D. Contreras, R. J. Candal, E. E. Sileo, and H. D. Mansilla, "Photocatalyzed degradation of flumequine by doped TiO_2 and simulated solar light," *Journal of Hazardous Materials*, vol. 155, no. 1-2, pp. 45–50, 2008.

[21] *NIST Chemistry WebBook*, http://webbook.nist.gov/chemistry/.

[22] P. M. Schaber, J. Colson, S. Higgins, D. Thielen, B. Anspach, and J. Brauer, "Thermal decomposition (pyrolysis) of urea in an open reaction vessel," *Thermochimica Acta*, vol. 424, no. 1-2, pp. 131–142, 2004.

[23] D. Mitoraj and H. Kisch, "The nature of nitrogen-modified titanium dioxide photocatalysts active in visible light," *Angewandte Chemie*, vol. 47, no. 51, pp. 9975–9978, 2008.

[24] D. Mitoraj and H. Kisch, "On the mechanism of urea-induced titania modification," *Chemistry*, vol. 16, no. 1, pp. 261–269, 2010.

[25] J. Buha, I. Djerdj, M. Antonietti, and M. Niederberger, "Thermal transformation of metal oxide nanoparticles into nanocrystalline metal nitrides using cyanamide and urea as nitrogen source," *Chemistry of Materials*, vol. 19, no. 14, pp. 3499–3505, 2007.

[26] D. Mitoraj, R. Beránek, and H. Kisch, "Mechanism of aerobic visible light formic acid oxidation catalyzed by poly(tri-s-triazine) modified titania," *Photochemical and Photobiological Sciences*, vol. 9, no. 1, pp. 31–38, 2010.

[27] P. Górska, A. Zaleska, and J. Hupka, "Photodegradation of phenol by UV/TiO_2 and Vis/N,C-TiO_2 processes: comparative mechanistic and kinetic studies," *Separation and Purification Technology*, vol. 68, no. 1, pp. 90–96, 2009.

[28] A. E. Regazzoni, P. Mandelbaum, M. Matsuyoshi, S. Schiller, S. A. Bilmes, and M. A. Blesa, "Adsorption and photooxidation of salicylic acid on titanium dioxide: a surface complexation description," *Langmuir*, vol. 14, no. 4, pp. 868–874, 1998.

[29] N. Wang, L. Zhu, Y. Huang, Y. She, Y. Yu, and H. Tang, "Drastically enhanced visible-light photocatalytic degradation of colorless aromatic pollutants over TiO_2 via a charge-transfer-complex path: a correlation between chemical structure and degradation rate of the pollutants," *Journal of Catalysis*, vol. 266, no. 2, pp. 199–206, 2009.